

# Ultrasensitive Detection of Bacteria Using Core–Shell Nanoparticles and an NMR-Filter System\*\*

Hakho Lee, Tae-Jong Yoon, and Ralph Weissleder\*

Direct detection of pathogens is key in combating human infections, in identifying nosocomial sources, in surveying food chains, and in biodefense.<sup>[1]</sup> Recent advances in nanotechnology have enabled the development of new diagnostic platforms<sup>[2]</sup> aimed at more sensitive and faster pathogen detection.<sup>[3]</sup> Many of the reported technologies, albeit elegant, often fail in routine clinical settings<sup>[4]</sup> because they still require extensive specimen purification, use complex measurement setups, or are not easily scalable for clinical demands. Here we report a new, simple, nanoparticle-based platform that can rapidly detect pathogens in native biological samples. In this approach, bacteria are targeted by highly magnetic nanoparticles (MNPs), concentrated into a microfluidic chamber, and detected by nuclear magnetic resonance (NMR). The clinical utility of our diagnostic platform was evaluated by detecting tuberculosis (TB), a leading cause of disease and death worldwide.<sup>[5]</sup> Using the bacillus Calmette-Guérin (BCG) as a surrogate for *Mycobacterium tuberculosis*, we demonstrate unprecedented detection speed and sensitivity; as few as 20 colony-forming units (CFU) in sputum (1 mL) were detected in less than 30 min. With the capability for fast and simple operation, and portable instrumentation, the new detection platform could be an ideal point-of-care diagnostic tool, especially in resource-limited settings.

The diagnosis starts with specimen collection and incubation with bacteria-specific magnetic nanoparticles (MNPs) (see Figure S1 in the Supporting Information). MNPs bind to the bacterial wall, rendering the bacteria superparamagnetic. In a subsequent step the spin–spin relaxation time ( $T_2$ ) of the whole sample is measured by NMR spectroscopy. As the magnetic fields from the MNPs dephase the precession of nuclear spins in water protons,<sup>[6,7]</sup> each MNP-tagged bacterium can shorten the  $T_2$  of billions of surrounding water

molecules. To increase detection sensitivity, we have incorporated signal amplification schemes that made it possible to detect small quantities of bacteria in relatively large sample volumes. At the nanoparticle level, the detection signal has been enhanced by synthesizing iron-based MNPs with high transverse relaxivity ( $r_2$ ). At the device level, the signal was amplified by concentrating bacteria in a microfluidic chamber where the NMR signal was measured. To provide portable, on-chip bacterial detection, the NMR signal was read out using a miniaturized NMR system we have recently developed.<sup>[8]</sup>

First, we developed hybrid MNPs with a large Fe core and a thin ferrite shell (“cannonballs”; CBs), which have very high  $r_2$  values per particle (see Table S1 in the Supporting Information). Owing to the limited number of binding sites per bacterium, the  $T_2$  of samples will be shorter and thereby the detection will be more sensitive when the individual MNPs have higher  $r_2$  values. Since  $r_2$  is proportional to  $M^2 d^2$ , where  $M$  and  $d$  are the particle magnetization and the diameter, respectively,<sup>[6]</sup> we focused on making larger MNPs using highly magnetic material (Fe). Figure 1a shows an example of highly monodisperse CBs ( $d = 16$  nm). Initially, we made Fe-only MNPs by thermally decomposing  $\text{Fe}(\text{CO})_5$ , and then oxidizing the particles in air to grow the ferrite shell.<sup>[9]</sup> Our method produces a thinner shell than that produced by chemical oxidation<sup>[10]</sup> and thereby leaves a larger Fe core (see Figure S2 in the Supporting Information), leading to higher magnetization. The shell showed high crystallinity (Figure 1b), and X-ray diffraction revealed a typical pattern for a spinel structure (Figure 1c), confirming the ferrite nature of the shell.<sup>[11]</sup> The shell protected the Fe core from oxidation to maintain the magnetic properties of the CBs (see Figure S3 in the Supporting Information). The CBs showed high magnetization ( $139 \text{ emu g}^{-1} [\text{Fe}]$ ) and yet were superparamagnetic at room temperature (Figure 1d). Most importantly, the CBs displayed high transverse relaxivity ( $6.1 \times 10^{-11} \text{ mL s}^{-1}$ , 1.5 T; see Figure S4 in the Supporting Information), as a result of their high magnetization and large diameter.


To render CBs specific for BCG, we conjugated anti-BCG monoclonal antibodies to their surface (CB-BCG; see Methods in the Supporting Information). Bacterial samples were then incubated with CB-BCG for 10 min and then washed to remove excess particles. Optical microscopy with fluorescent CB-BCG showed excellent targeting (Figure 2a). The binding of CB-BCG was further verified by the element mapping (Figure 2b), which showed a high Fe signal on the bacterial membrane. The number of CB-BCG particles per bacterium, quantified by inductively coupled plasma atomic emission spectroscopy (ICP-AES; see Figure S5 in the

[\*] Prof. Dr. R. Weissleder  
Department of Systems Biology, Harvard Medical School  
200 Longwood Avenue, Boston, MA 02115 (USA)  
Fax: (+1) 617-643-6133  
E-mail: rweissleder@mgh.harvard.edu

Dr. H. Lee,<sup>[†]</sup> Dr. T. Yoon,<sup>[†]</sup> Prof. Dr. R. Weissleder  
Center for Systems Biology  
Massachusetts General Hospital/Harvard Medical School  
185 Cambridge Street, Boston, MA 02114 (USA)

[†] These authors contributed equally.

[\*\*] We thank D. Hung (MGH) and M. Cima (MIT) for many helpful discussions, R. M. Westervelt (Harvard) for support in device fabrication, and N. Sergeyev (MGH) for synthesizing CLIO. This work was supported by U01 HL080731.

 Supporting information for this article (including details on the experimental method) is available on the WWW under <http://dx.doi.org/10.1002/anie.200901791>.

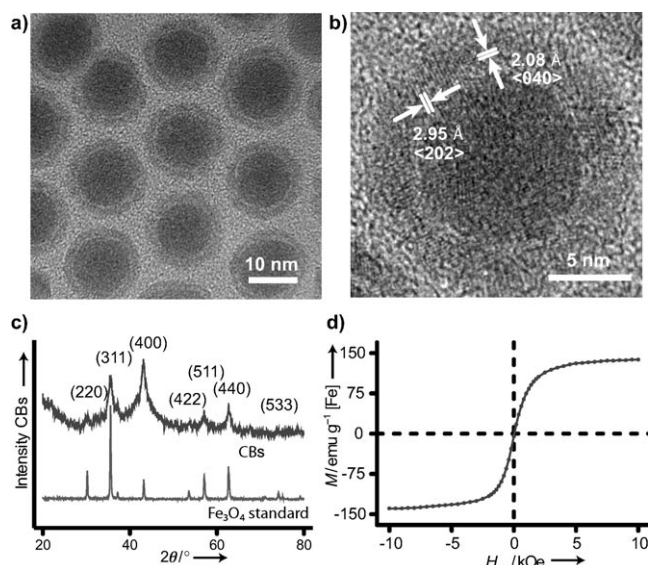


**Figure 1.** Cannonballs (CBs) for bacterial targeting. a) The particles have a large metallic core (Fe) passivated with a thin ferrite shell, resulting in high particle relaxivity ( $> 5 \times 10^{-11}$  mL s $^{-1}$  at 0.5 T). The core diameter and the shell thickness are 11 and 2.5 nm, respectively. CBs are highly monodisperse and well-suspended in solution. b) High-resolution image of a CB showing the crystallinity of the iron oxide shell with lattice constants. The shell consists of multiple domains of single crystals as a result of the lattice mismatch between the iron oxide shell and Fe core. c) The X-ray powder diffractogram of CBs reveals a typical spinel structure like that in the Fe<sub>3</sub>O<sub>4</sub> standard, verifying the ferrite nature of the shell. The relatively high intensity at the (400) position is attributed to the overlapping of the (100) peak from the Fe core. d) CBs (diameter of 16 nm) had high saturation magnetization ( $\approx 139$  emu g $^{-1}$  [Fe]), but were superparamagnetic at 300 K.  $H_{ex}$ : external magnetic field strength.

Supporting Information), was on the order of  $10^5$ . Magnetic tagging thus made the bacteria highly efficient  $T_2$ -shortening agents (Figure 2c). The binding of CB-BCG to BCG could be inhibited by antibody blockade against bacterial epitopes. For control CB or when CB-BCG was used against other bacterial strains, the CB binding was minimal with  $T_2$  changes ( $\Delta T_2$ )  $< 5\%$ . The number of CB-BCG units tested against different bacteria species were less than 600 per bacterium (see Figure S5 in the Supporting Information), confirming the specificity of CB-BCG.

To further enhance detection sensitivity and to streamline assay procedures, we next developed a chip-based filter system with NMR compatibility (Figure 3). A key component is a microfluidic chamber enclosed by a membrane filter and surrounded by a microcoil. The membrane filter performs two functions. First, it captures bacteria and concentrates them into the microfluidic chamber for NMR detection, providing a way to detect a small number of bacteria from large sample volumes. Second, the filter enables on-chip separation of bacteria from unbound CBs, obviating the need for separate off-chip purification steps. Figure 4a illustrates the operating principle of the NMR-filter system. An unpurified sample is introduced into the microfluidic channel. Bacteria are retained by the membrane (pore size  $\approx 100$  nm), while excess CBs permeate. Subsequently, a buffer solution is

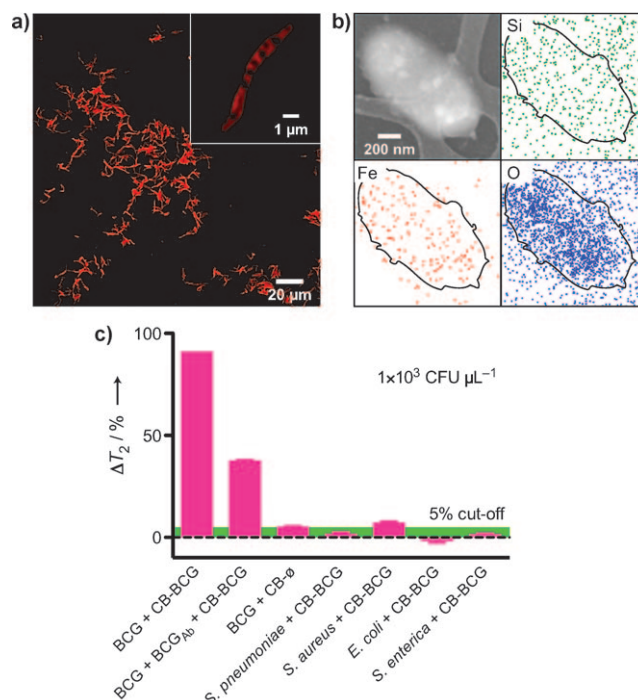


**Figure 2.** Selective BCG targeting with CB-BCG. a) Confocal micrograph of BCG incubated with fluorescently labeled CB-BCG. b) Transmission electron micrograph of BCG targeted with CB-BCG. Element mapping detected a high Fe signal on a whole bacterium. c) Specificity of CB-BCG. A panel of different bacteria samples were prepared as indicated ( $\approx 10^3$  CFU  $\mu$ L $^{-1}$ ) and NMR measurements were performed. The BCG sample incubated with CB-BCG showed large  $T_2$  changes ( $\Delta T_2$ ), whereas control samples had  $\Delta T_2 < 5\%$ . CB-∅: unmodified CB, BCG<sub>Ab</sub>: anti-BCG monoclonal antibody.

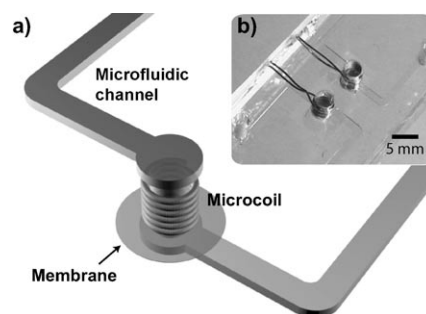


**Figure 3.** NMR-filter system for bacterial concentration and detection. a) The system consists of a microcoil and a membrane filter integrated with a microfluidic channel; the microcoil is used for NMR measurements; the membrane filter concentrates bacteria inside the NMR detection chamber to achieve high detection sensitivity. b) A prototype device with two measurement sites. The NMR detection volume was  $\approx 1$   $\mu$ L.

repeatedly injected to wash off unbound CBs and the membrane is backwashed to redisperse the captured bacteria. Figure 4b shows an operation example with a sample containing BCG and CB-BCG. After sample loading, the microfluidic channel was flushed with phosphate-buffered saline (PBS) to remove unbound CB-BCG. Finally, the flow

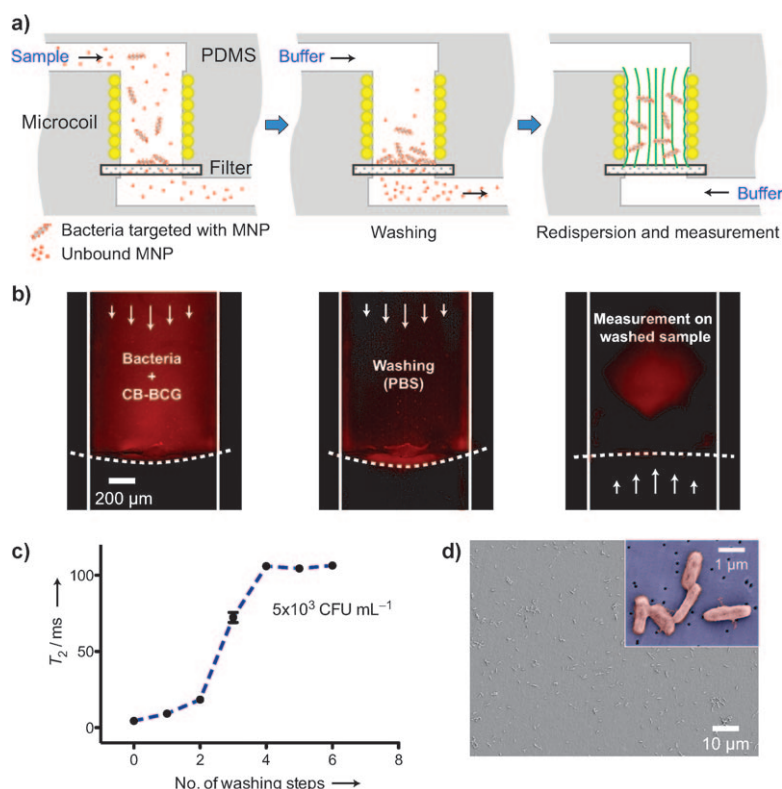


**Figure 4.** Bacterial separation and concentration. a) The unprocessed sample containing bacteria and CB-BCG is introduced into the device. The membrane filter retains bacteria while unbound CB-BCG pass through. To remove free CB-BCG, the microfluidic channel is repeatedly flushed with buffer. Finally, the flow is reversed to redisperse the captured bacteria and NMR measurements are performed. b) Demonstration of bacteria capture. A device without a microcoil was used for optical microscopy. c) The ideal number of wash steps to remove unbound CB was determined. Following each wash with PBS (100  $\mu$ L), the sample was redispersed and NMR measurements were performed. Note that  $T_2$  reached a plateau after 4 washes. d) After the final wash step, the membrane filter was imaged to confirm bacterial capture.

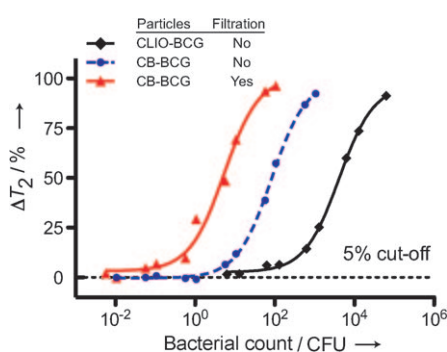


**Figure 5.** Comparison of detection sensitivity. Measurements were performed on samples with varying BCG counts to determine detection sensitivities. First, a microfluidic chip without a membrane filter was used to determine the intrinsic mass-detection limits. The bacteria were targeted either with CB-BCG or CLIO-BCG. With CB-BCG, we already achieved a mass-detection limit of  $\approx 6$  CFU (1  $\mu$ L detection volume), much lower than that of  $\approx 100$  CFU for CLIO-BCG. When CB-BCG-targeted samples (100  $\mu$ L) were filtered, the concentration limit was further reduced to  $\approx 60$  CFU mL<sup>-1</sup>.

direction was reversed to resuspend the captured BCG for NMR measurements. The number of washing steps to remove unbound CB-BCG was determined by measuring  $T_2$  after each wash (Figure 4c).  $T_2$  values plateaued after four to five washing steps, with the whole washing procedure complete in less than 5 min. The electron micrograph of the membrane after complete wash (Figure 4d) verified bacterial capture on the filter. Note that by removing unbound particles, CB-induced  $T_2$  changes are much more pronounced than the previously described homogeneous assay<sup>[8]</sup> and the detection sensitivity is increased by  $> 10^3$ .

To compare the effect of MNP relaxivity on detection sensitivity, we first used an NMR system without a membrane filter. Two types of nanoparticles, CBs and cross-linked iron oxide<sup>[12]</sup> (CLIO;  $r_2 = 7.0 \times 10^{-13}$  mL s<sup>-1</sup>), were used (Figure 5, black and blue curves). CB-BCG showed much higher mass sensitivity, detecting as few as six colony-forming units (CFU) (in 1  $\mu$ L sample volume), whereas the detection limit was approximately 100 CFU with CLIO-BCG. Using the NMR-filter system, we achieved substantially high concentration detection sensitivity (Figure 5, red curve). When BCG samples (100  $\mu$ L) targeted with CB-BCG were filtered, the concentration detection limit was roughly 60 CFU mL<sup>-1</sup>. It is important to note that the concentration limit is theoretically unlimited with the filtering, because bacteria can be concentrated into the NMR detection chamber from large sample volumes.

To evaluate the clinical utility of the NMR-filter system, we performed comparative detection assays (see Table S3 in the Supporting Information). Pulmonary samples were prepared by spiking BCG into human sputa. Following liquefaction, samples were subjected to standard TB diagnostic tests, culture and acid-fast bacilli (AFB) smear microscopy, and CB-based NMR measurements. Without filtration, NMR measurements were as sensitive as AFB smear microscopy, with a detection threshold of about  $10^3$  CFU mL<sup>-1</sup>. However, the NMR method was less prone to human error and less labor-intensive. With the NMR-filter system, the detection sensitivity was comparable to that of culture-based detection; when 1 mL of samples were filtered, the detection limit was  $\approx 20$  CFU. The NMR-based detection was much faster ( $< 30$  min) and was performed on a single microfluidic chip, in marked contrast with the culture-based test that was time-consuming ( $> 2$  weeks) and facility-dependent (e.g. incubators). These results demonstrate that the CB-based NMR-filter system can be readily applied for TB diagnosis in clinical settings.<sup>[13]</sup>

Received: April 2, 2009

Published online: June 24, 2009

**Keywords:** biosensors · microfluidics · nanoparticles · nanotechnology · NMR spectroscopy

- [1] a) C. Batt, *Science* **2007**, *316*, 1579; b) M. Enserink, *Science* **2001**, *294*, 1266; c) M. Struelens, O. Denis, H. Rodriguez-Villalobos, *Microbes Infect.* **2004**, *6*, 1043.
- [2] a) P. Luo, F. Stutzenberger, *Adv. Appl. Microbiol.* **2008**, *63*, 145; b) N. Rosi, C. Mirkin, *Chem. Rev.* **2005**, *105*, 1547.
- [3] a) H. Grossman, W. Myers, V. Vreeland, R. Bruehl, M. Alper, C. Bertozzi, J. Clarke, *Proc. Natl. Acad. Sci. USA* **2004**, *101*, 129; b) R. Phillips, O. Miranda, C. You, V. Rotello, U. Bunz, *Angew. Chem.* **2008**, *120*, 2628; *Angew. Chem. Int. Ed.* **2008**, *47*, 2590; c) X. Zhao, L. Hilliard, S. Mechery, Y. Wang, R. Bagwe, S. Jin, W. Tan, *Proc. Natl. Acad. Sci. USA* **2004**, *101*, 15027.
- [4] M. Urdea, L. Penny, S. Olmsted, M. Giovanni, P. Kaspar, A. Shepherd, P. Wilson, C. Dahl, S. Buchsbaum, G. Moeller, D. Hay Burgess, *Nature* **2006**, *444*, 73.
- [5] E. Keeler, M. Perkins, P. Small, C. Hanson, S. Reed, J. Cunningham, J. Aledort, L. Hillborne, M. Rafael, F. Giroi, C. Dye, *Nature* **2006**, *444*, 49.
- [6] R. Brooks, *Magn. Reson. Med.* **2002**, *47*, 388.
- [7] J. Perez, L. Josephson, T. O'Loughlin, D. Hogemann, R. Weissleder, *Nat. Biotechnol.* **2002**, *20*, 816.
- [8] H. Lee, E. Sun, D. Ham, R. Weissleder, *Nat. Med.* **2008**, *14*, 869.
- [9] A. Cabot, V. Puentes, E. Shevchenko, Y. Yin, L. Balcells, M. Marcus, S. Hughes, A. Alivisatos, *J. Am. Chem. Soc.* **2007**, *129*, 10358.
- [10] S. Peng, C. Wang, J. Xie, S. Sun, *J. Am. Chem. Soc.* **2006**, *128*, 10676.
- [11] F. Jiao, J. Jumas, M. Womes, A. Chadwick, A. Harrison, P. Bruce, *J. Am. Chem. Soc.* **2006**, *128*, 12905.
- [12] L. Josephson, C. H. Tung, A. Moore, R. Weissleder, *Bioconjugate Chem.* **1999**, *10*, 186.
- [13] M. Perkins, *Int. J. Tuberc. Lung Dis.* **2000**, *4*, S182.